UC Davis
UC Davis Previously Published Works

Title

A large-scale screen reveals genes that mediate electrotaxis in Dictyostelium discoideum

Permalink

https://escholarship.org/uc/item/8rx866r1

Journal

Science Signaling, 8(378)

ISSN

1945-0877

Authors

Gao, Runchi

Zhao, Siwei

Jiang, Xupin

et al.

Publication Date

2015-05-26

DOI

10.1126/scisignal.aab0562

Copyright Information

Peer reviewed

CELL MIGRATION

A large-scale screen reveals genes that mediate electrotaxis in *Dictyostelium discoideum*

Runchi Gao,[1,2,3] Siwei Zhao,[4]* Xupin Jiang,[5]* Yaohui Sun,[2] Sanjun Zhao,[1,2] Jing Gao,[1,2] Jane Borleis,[3] Stacey Willard,[3] Ming Tang,[3] Huaqing Cai,[3] Yoichiro Kamimura,[3] Yuesheng Huang,[5] Jianxin Jiang,[5] Zunxi Huang,[1] Alex Mogilner,[6] Tingrui Pan,[4] Peter N. Devreotes,[3] Min Zhao[2†]

Directional cell migration in an electric field, a phenomenon called galvanotaxis or electrotaxis, occurs in many types of cells, and may play an important role in wound healing and development. Small extracellular electric fields can guide the migration of amoeboid cells, and we established a large-scale screening approach to search for mutants with electrotaxis phenotypes from a collection of 563 *Dictyostelium discoideum* strains with morphological defects. We identified 28 strains that were defective in electrotaxis and 10 strains with a slightly higher directional response. Using plasmid rescue followed by gene disruption, we identified some of the mutated genes, including some previously implicated in chemotaxis. Among these, we studied *PiaA*, which encodes a critical component of TORC2, a kinase protein complex that transduces changes in motility by activating the kinase PKB (also known as Akt). Furthermore, we found that electrotaxis was decreased in mutants lacking *gefA*, *rasC*, *rip3*, *lst8*, or *pkbR1*, genes that encode other components of the TORC2-PKB pathway. Thus, we have developed a high-throughput screening technique that will be a useful tool to elucidate the molecular mechanisms of electrotaxis.

INTRODUCTION

More than 100 years ago, Verworn observed that amoebae migrated directionally in extracellular electric fields—a phenomenon termed galvanotaxis (or electrotaxis) (*1–3*). Electrotaxis toward the cathode was reported later in several species of slime molds, including the plasmodium *Physarum polycephalum* (*1*, *4*). Subsequently, many types of cells, from bacteria and yeast to mammalian cells, including skin keratinocytes and corneal epithelial cells, polarize and migrate directionally in electric fields (*5–16*), even though many of these nonneuronal cells would not be expected to experience electric fields in their natural environments. However, naturally occurring endogenous fields have been detected during development and wound healing. In wounds, electric fields with strengths of 100 to 150 mV/mm have been measured, with the wound center being more negative relative to the surrounding tissues. The endogenous fields thus have been suggested as a physiological signal that polarizes cells and guides cell migration (*11*, *17–24*). Furthermore, migrating giant amoeba cells produce membrane-controlled electrical currents that correlate with the direction of cell movement (*25*), and during mound formation in multicellular aggregates, small electric currents can be measured (*26*).

Our understanding of electrotaxis is rudimentary and fragmented, compared to our understanding of chemotaxis, due largely to the absence of a genetically tractable model organism and an effective approach to characterize electrotaxis phenotypes. In mammalian cells, the opening of voltage-gated ion channels has been hypothesized to play a role in electrotaxis, because applied electric fields induce hyperpolarization of the membrane

potential on the anodal side and depolarization on the cathodal side of cells. Electrostatic and electroosmotic forces at the plasma membrane exert mechanical forces on the cell and redistribute the charged components of the membrane, which may facilitate the establishment of a cathodal-anodal axis of polarity (*12*, *27*, *28*). Ion channels and pathways containing signaling proteins such as epidermal growth factor receptors, integrins, protein kinase A, mitogen-activated kinases, and PI3K/PTEN (phosphoinositide 3-kinases/phosphatase and tensin homolog) can mediate electrotaxis (*10*, *20*, *29–32*). Currently available technology for electrotaxis experiments allows analysis of only a limited number of strains or types of cells or drug treatments, and normally, only one strain or treatment can be tested at a time. A more powerful genetic approach with increased throughput could greatly advance the field. Because *Dictyostelium discoideum* is genetically amenable and actively motile, it has been a powerful model organism for chemotaxis. Studies using *Dictyostelium* have produced substantial mechanistic insights into the signaling mechanisms underlying cell polarity and migration. In addition, we and others have previously demonstrated robust electrotaxis in *Dictyostelium* cells (*5*, *33*, *34*), although little is known about the mechanism except that it is G protein (heterotrimeric guanine nucleotide–binding protein)–independent and can be reversed by genetically modulating both guanylyl cyclases and cyclic guanosine monophosphate (cGMP)–binding protein C in combination with inhibition of PI3Ks (*34*). Here, we established a high-throughput screening technique for electrotaxis phenotypes. Serendipitously, we had previously found a spontaneous mutant strain that had lost the electrotactic response, and which also displayed a defect in developmental patterning. Therefore, we decided to screen from a collection of developmentally defective strains of *Dictyostelium* cells as an initial test of the technique. Because many chemotaxis mutants also display developmental defects, we reasoned that the screen could also reveal common and distinct requirements for electrotaxis and chemotaxis.

From this screen, we identified genes that are involved in electrotaxis including the *pianissimo* (*PiaA*) gene. Originally isolated as a chemotaxis gene, *Pia*A is a key subunit of the TORC2 complex. In *Dictyostelium*, PiaA plays a critical role in stimulating adenylyl cyclase (ACA) and in activating protein kinase B (PKB) in addition to its role in chemotaxis (*35*, *36*). We quantitatively delineated the roles of other molecular components

[1]School of Life Sciences, Yunnan Normal University, Kunming, Yunnan 650500, China. [2]Departments of Dermatology and Ophthalmology, Institute for Regenerative Cures, School of Medicine, University of California at Davis, Davis, CA 95817, USA. [3]Department of Cell Biology and Anatomy, Johns Hopkins University, School of Medicine, Baltimore, MD 21205, USA. [4]Department of Biomedical Engineering, University of California at Davis, Davis, CA 95616, USA. [5]State Key Laboratory of Trauma, Burns and Combined Injury, Third Military Medical University, Chongqing 400042, China. [6]Courant Institute and Department of Biology, New York University, 251 Mercer Street, New York, NY 10012, USA.
*These authors contributed equally to this work.
†Corresponding author. E-mail: minzhao@ucdavis.edu

Fig. 1. High-throughput screen determined electrotaxis phenotypes. (A) Compiled electrotaxis phenotypes of 563 strains from the mutant collection, arranged according to directedness value. The red rectangle on the left end shows severely defective strains, and that on the right shows the hyperresponsive mutants. WT, wild type. (B) Mutant cells were categorized into four groups according to the directedness value cos θ. Normal electrotaxis group: strains with cos θ between 0.5 and 0.9, accounting for 68% of the collection screened; low electrotaxis group: those with cos θ between 0.3 and 0.5, accounting for 24% of the collection; defective electrotaxis group: those with cos θ less than 0.3, accounting for 5% of the collection; hyperresponsive group: those with cos θ higher than 0.9, accounting for 3% of the collection. (C and D) Examples of defective and hyperresponsive strains. Labels of the x axis indicate strain codes. Results shown are from experiments with an electric field (EF) of 12 V/cm. Data are means ± SEM from at least 50 cells per strain from three independent experiments. *$P < 0.05$, **$P < 0.01$, Student's t test, compared with AX2 WT cells in an electric field of the same strength. (E) Representative trajectories of typical strains from WT, defective, and hyperresponsive groups. Plots show migration paths of multiple cells with the start position of each cell centered at point 0,0. Field strength and polarity are as shown.
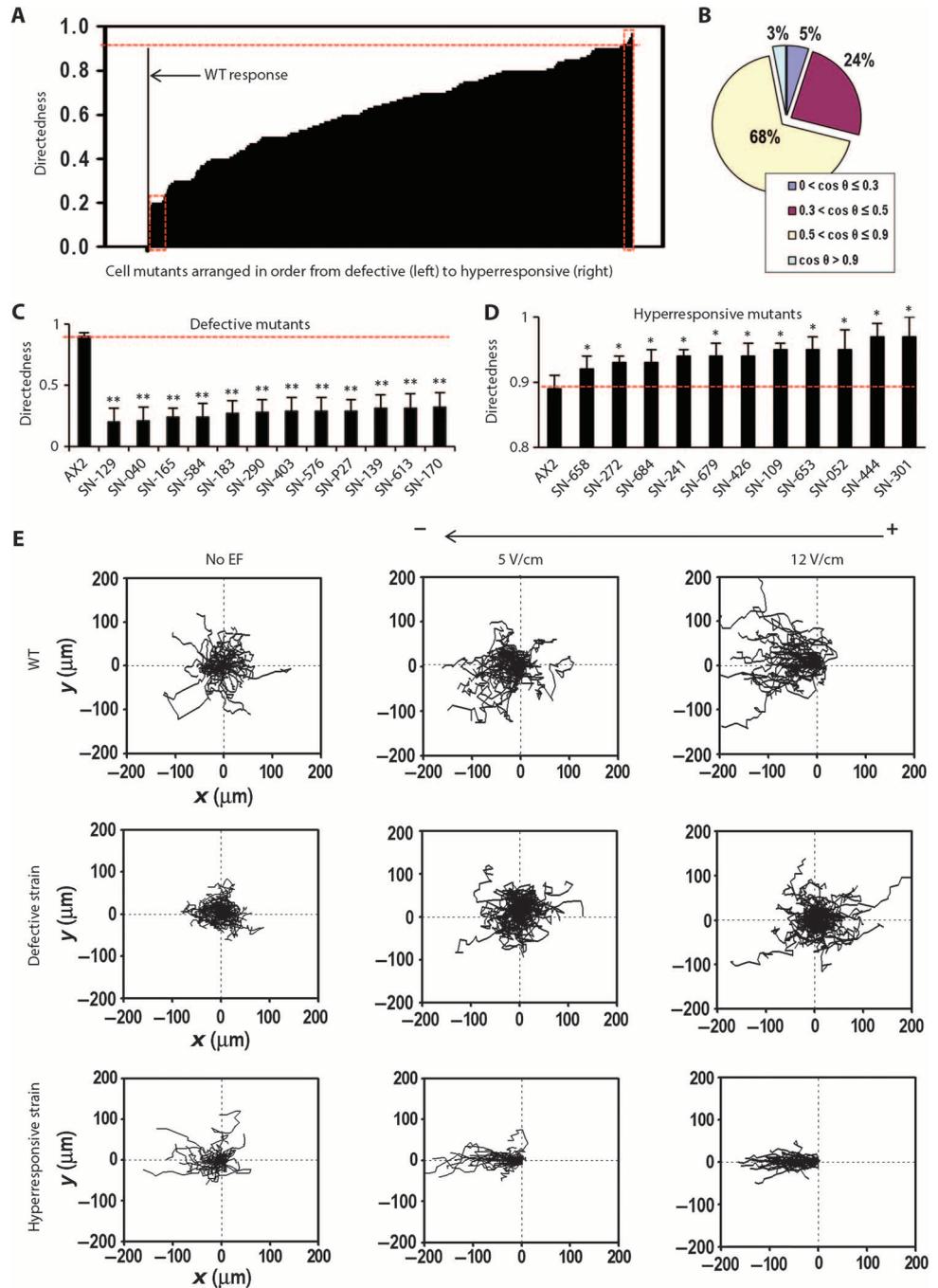
of the TORC2 pathway in electrotaxis and found that *GefA*, *RasC*, TORC2 (*Rip3*, *Lst8*), and *PKBR1* were critical for electrotactic responses. We thus demonstrated the feasibility and robustness of the screening technique to investigate electrotaxis in a large number of different mutant strains. In conjunction with our high-throughput technique, *Dictyostelium* is an excellent model to identify critical signaling molecules and to map the signaling pathways underlying electrotaxis. This screening technique can be adapted to other types of cells and offers a powerful strategy to identify electrotaxis phenotypes within large collections of cells.

RESULTS

Establishment of a collection of mutants with developmental defects

We established a collection of mutant strains of *Dictyostelium* with developmental defects using restriction enzyme–mediated integration (REMI) on the wild-type strains AX2 and AX3, and morphology screening (fig.

S1) (*37–39*). A total of 710 morphologically defective mutants were isolated from a REMI library provided by R. Kay. Specifically, these mutants were defective in aggregation, streaming, mound formation, stalk or spore formation, culmination, or fruiting body formation (fig. S1). Because the library had been amplified, the repeated isolations do not imply that the screens were saturated, and we could not estimate the number of involved genes. Nevertheless, there was sufficient diversity in the library and within the collection of developmental mutants to identify a group of genes involved in electrotaxis.

Barcoded microplates for high-throughput electrotaxis screening

To efficiently screen a large number of mutant strains, we developed a high-throughput screening method centered on barcoded microplates to enable us to conduct electrotaxis experiments and assays on many samples at the same time (figs. S2 and S3). We loaded a large number of individual mutant strains onto separate microplates, with each mutant strain identified by a unique barcode (fig. S2A). We then mixed the microplates and loaded them into an electrotaxis chamber and subjected them to a global electric field. We recorded cell migration using digital video imaging and analyzed each individual microplate. Microplates with different strains were mixed and mounted in the same electrotaxis chamber; however, a benefit of optical machine-readable barcodes is that they allow the experimenter to identify individual strains using the unique barcode assigned (figs. S2, B and C, S3).

To facilitate the screen, we optimized protocols to prepare cells for electrotaxis experiments. We seeded cells on the plates in nonnutrient development buffer and quantified electrotaxis at different time points. Growing (vegetative) cells displayed electrotaxis with directedness values significantly higher than control cells not subjected to an electric field, albeit weaker than cells that were optimally developed for the most efficient chemotactic response to cAMP (adenosine 3′,5′-monophosphate) by pulsing with cAMP for 5 hours (5, 34). Directedness is an index that measures the extent of the alignment of cell movement with field direction. The directedness of cell migration was assessed as cosine θ, where θ is the angle between the electric field vector and a straight line connecting the start and end positions of a cell. An average directedness value of 1 would indicate that 100% of the cells moved perfectly directionally to the cathode, whereas a directedness value of 0 indicates random migration (5, 20). At 3 hours of starvation in the development buffer without cAMP pulsing (Materials and Methods), the directedness value was 0.8. We used cells after 3 hours of starvation for all experiments unless stated otherwise (Fig. 1A). There were no significant differences in the electrotactic responses between the wild-type strains AX2 and AX3 (fig. S8).

We confirmed that introduction of the microplates into the electrotaxis chamber did not affect overall electrotaxis when plates were placed in different positions in the chamber (fig. S4). We also verified that the cells on the microplates displayed the same electrotaxis parameters as previously determined on the tissue culture dishes, thus indicating that our results could be consistent with published results of electrotaxis of *Dictyostelium* cells on plastic culture dishes (fig. S5).

Identification of strains with electrotaxis phenotypes

To characterize directional migration, we measured trajectory speed, displacement speed, and persistency together with directedness (5, 20). The trajectory speed is the total length traveled (trajectory length) by the cells divided by time, and the displacement speed is the straight-line distance (displacement distance) between the start and end positions of a cell divided by time. Persistency is the ratio of displacement distance to trajectory length traveled by a cell, and indicates whether a cell migrated "directly" or had a more "wandering" (or tortuous) pathway (figs. S4, S5, and S8) (see Materials and Methods for details).

Using the directedness value, we grouped the screened cells into four subpopulations: wild type–like, moderately defective, severely defective, and hyperresponsive strains (Fig. 1, A and B). The wild type–like group had a directedness value of 0.5 to 0.9 and comprised 68% of the strains. The moderately defective group had directedness values of 0.3 to 0.5 and comprised 24% of the collection. The severely defective group had directedness values of less than 0.3 and comprised 5% of the strains (Fig. 1, B and C). The hyperresponsive strains had directedness values of

greater than 0.9, which were significantly higher than those of wild-type cells, and they comprised 3% of the strains (Fig. 1, B and D). Trajectories of cells pooled as composite graphs show the typical directional migration of the wild type–like, severely defective, and hyperresponsive cells at different voltages (Fig. 1E).

A decrease in directedness generally coincided with a decrease in persistency (Fig. 2, A and B), but did not always coincide with a decrease in migration speed (Fig. 2, C and D). For example, seven mutants with significantly decreased directedness showed increased migration speed (for example, strain code SN-183; Fig. 2C). Furthermore, hyperresponsive mutants did not consistently display an increased migration speed (table S2). These results suggest that defective and hyperresponsive phenotypes were not purely due to changes in motility.

Insertion sites and genes affected

We determined the insertion sites for 28 defective strains (Table 1 and tables S1 and S2). Five groups of genes were implicated according to the insertion sites. Six mutant strains had an insertion site within the *piaA* gene; four mutant strains had insertion sites between the *mybI* and *cmfB* genes; two strains contained insertions near the *cldA* and *rsg13* genes; other genes containing internal or nearby insertion sites include *qrt1*, *amdA*, *nat10*, *DDB_G0288175*, *DDB_G0278163*, and *abcA3*. We found that 12 strains deficient in one of these genes (table S3) showed electrotactic
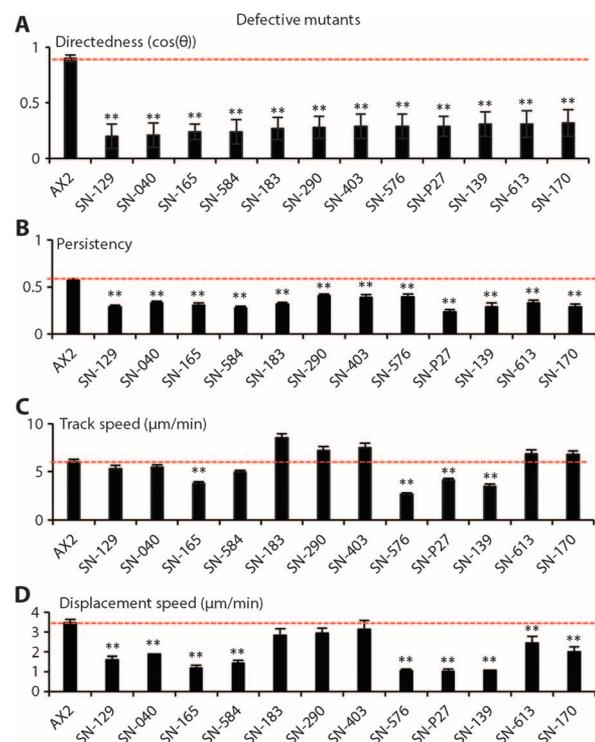

Fig. 2. Quantitative analyses of electrotactic responses in selective defective mutants. (**A**) Directedness values in selected severely defective strains. (**B**) Defective strains showed decreased migration persistence. (**C** and **D**) Migration speeds in the strains with significantly decreased directedness values. Data are means ± SEM from at least 50 cells per strain from three independent experiments in an electric field of 12 V/cm. Labels of the *x* axis indicate strain codes. *$P < 0.05$, **$P < 0.01$, Student's *t* test, compared with AX2 WT cells in an electric field of the same strength.

defects (figs. S6 and S7), thus confirming that these genes were involved in electrotaxis. The results are consistent with those from the screen of the collection of mutants with developmental defects (Table 1 and figs. S6 to S8).

Pianissimo as a key mediator of electrotaxis

We next focused on the *piaA* gene because its disruption produced a strong and consistent phenotype and its role in chemotaxis has been well characterized (Table 1). The *piaA⁻* cells are deficient in aggregation because they do not generate intercellular cAMP signals and are defective in chemotaxis (*35*) (Fig. 3A). All six isolates, which may be sister clones because the library was amplified, showed severe electrotactic defects with low directedness values around ~0.24 (Table 1 and table S1). We confirmed a role for *piaA* in electrotaxis with a strain in which the gene was disrupted by homologous recombination (Table 1 and Fig. 3B). The defective phenotype in *piaA⁻* cells was significantly decreased at all voltages tested up to 20 V/cm (Fig. 3, B to D). We expressed Flag-tagged *PiaA* in *piaA⁻* cells, which rescued the developmental defects as evidenced by the formation of fruiting bodies (Fig. 3A). In addition, electrotactic responses were restored in *piaA⁻* cells reexpressing *PiaA* (Fig. 3, B to D). As a control, *piaA⁻* cells expressing vector only (*pJK1/piaA⁻*) retained developmental and electrotactic defects (Fig. 3, A to C).

To exclude the possibility that developmental defects of *piaA⁻* cells resulted in the electrotaxis phenotype of these cells, we examined growing cells and tested whether inhibitors of TORC2 could acutely inhibit the electrotactic responses of 3-hour stage cells. For 3-hour stage cells, growing *piaA⁻* cells had significantly lower directedness compared to growing parental AX2 cells (fig. S7). Further, electrotaxis in 3-hour stage wild-type cells was impaired by the TORC2 inhibitor pp242 (Fig. 4, A and B), which inhibits TORC2-mediated phosphorylation of PKBR1 (*36, 40*), suggesting that PiaA mediates electrotaxis as a component of TORC2.

We next focused on the pathway in which PiaA is a critical component. TORC2 is activated at the leading edge of the cell, where it causes the localized activation of PKBs and phosphorylation of PKB substrates. In chemotaxis, RasC and its upstream activator, the guanine nucleotide exchange factor GefA, are upstream of TORC2 (*36, 41, 42*). TORC2 has two additional components, Lst8 and Rip3, which also play a role in chemotaxis. Furthermore, knockdown of Rictor, the mammalian ortholog of PiaA, compromises neutrophil chemotaxis (*43*). Disruption of *gefA*, *rasC*, *rip3*, *lst8*, *pkbA*, and *pkbR1* consistently suppressed electrotaxis, but to varying degrees (Fig. 4, C to F). Similar to *piaA⁻* cells, *rip3⁻* cells displayed a significantly decreased response, with a large decrease in directedness as well as in migration speed. The deletion strains *lst8⁻* and *pkbA⁻*, however, displayed less obvious electrotactic defects, whereas *pkbR1* deficiency appeared to have more significant effects on electrotaxis. Similar differences in the effects of this series of genes have been observed for chemotaxis (*36, 41, 44, 45*). As before, to exclude the possibility that the interaction between different mutants with the materials of barcoded microplate

Table 1. Strains that were severely defective in electrotaxis. Data are means ± SEM from at least 50 cells from three independent experiments.

| Strains	Electrotaxis index	Morphological defect	Chromosome: insertion site	Genes	Gene product
SN-129	(−)0.08 ± 0.02	Streamer	5:2430559	*mybI; cmfB*	myb domain–containing protein; putative CMF receptor CMFR1
SN-576	(−)0.16 ± 0.02	Mound	3:1355756	*cldA;RGS13*	Clu domain–containing protein A; regulator of G protein signaling 13
SN-183	(−)0.17 ± 0.02	Agg-	2:8027355	*piaA*	Cytosolic regulator of ACA; alternative protein name is Pianissimo
SN-494	(−)0.19 ± 0.03	Fuzzy	6:771404	*qtrt1*	Queuine tRNA-ribosyltransferase
SN-517	(−)0.20 ± 0.03	Mound	1:4688833	*DDB_G0270350_ps*	Pseudogene
SN-028	(−)0.21 ± 0.05	Mound	6:1494014	*amdA*	AMP deaminase
SN-447	(−)0.21 ± 0.04	Mound	1:2285000	*nat10*	Putative *N*-acetyltransferase
SN-613	(−)0.22 ± 0.05	Mound	6:1494014	*amdA*	AMP deaminase
SN-677	(−)0.22 ± 0.04	Mound	1:2285000	*nat10*	Putative *N*-acetyltransferase
SN-123	(−)0.22 ± 0.04	Mound	6:2664855	*DDB_G0293234*	*N*-acetyltransferase, noncatalytic subunit
SN-P27	(−)0.23 ± 0.05	Agg-	5:2430475	*mybI; cmfB*	Same as above
SN-139	(−)0.24 ± 0.05	Agg-	2:8027355	*piaA*	Same as above
SN-150	(−)0.24 ± 0.03	Agg-	2:8027355	*piaA*	Same as above
SN-333	(−)0.25 ± 0.02	Agg-	5:1156568	*DDB_G0288175*	UV radiation resistance–associated gene protein (automated)
SN-598	(−)0.20 ± 0.04	Agg-	5:2430475	*mybI; cmfB*	Same as above
SN-584	(−)0.20 ± 0.06	Stramer	3:388181	*DDB_G0278163*	TM2 domain–containing protein
SN-106a	(−)0.21 ± 0.04	Agg-	2:8027355	*piaA*	Same as above
SN-040	(−)0.21 ± 0.07	Agg-	3:389227	*tgrA_ps8*	Pseudogene
SN-xxx	(−)0.23 ± 0.03	Agg-	3:388181	*DDB_G0278163*	TM2 domain–containing protein
SN-165	(−)0.24 ± 0.07	Agg-	2:8013514	*DDB_G0277539*	WEE family protein kinase DDB_G0277539
SN-661	(−)0.25 ± 0.03	Culmination	3:1355756	*cldA;DDB_G0278897*	Clu domain–containing protein A; regulator of G protein signaling 13
SN-242	(−)0.26 ± 0.05	Agg-	2:8027893	*piaA*	Same as above
SN-252	(−)0.27 ± 0.04	Mound	1:4688833	*DDB_G0270350_ps*	Pseudogene
SN-223	(−)0.28 ± 0.05	Agg-	2:8027355	*piaA*	Same as above
SN-290	(−)0.28 ± 0.04	Streamer	5:2430475	*mybI; cmfB*	Same as above
SN-432	(−)0.29 ± 0.06	Mound	5:2430475	*mybI; cmfB*	Same as above
SN-403	(−)0.29 ± 0.05	Fuzzy	5:2430475	*mybI; cmfB*	Same as above
SN-170	(−)0.29 ± 0.04	Agg-	6:2879930	*abcA3*	ABC transporter A family protein
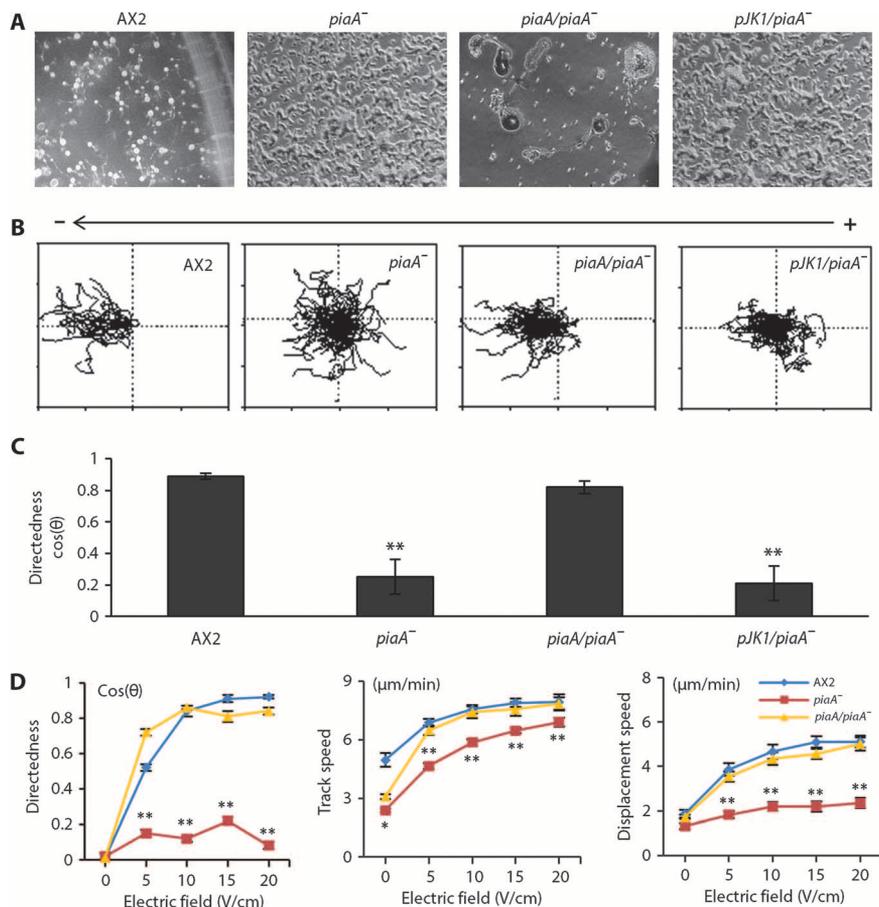
Fig. 3. PiaA is essential for electrotaxis in *D. discoideum*. Null mutation of *piaA* significantly reduced electrotaxis, which was rescued by reexpression of piaA. (**A**) *piaA⁻* cells displayed an aggregation defect, which was rescued by reexpression of *piaA*. WT, *piaA⁻*, *Flag-piaA/piaA⁻* (*piaA/piaA⁻*), and *pJK1/piaA⁻* cells were developed on nonnutrient agar plates and photographed at 48 hours. (**B**) Trajectories of cells in an electric field of 12 V/cm. The square is 200 μm × 200 μm. Polarity is as shown. (**C**) Directedness values of the four strains in an electric field. (**D**) *PiaA⁻* cells showed a significant defect in electrotaxis at all voltages tested. *Flag-piaA/piaA⁻* cells showed normal electrotaxis at all voltages. See also movies S1 to S4. Data are means ± SEM from at least 50 cells per genotype from three independent experiments. *$P < 0.05$, **$P < 0.01$, Student's *t* test, compared with AX2 WT cells.

affected electrotaxis assessment, we cultured knockout cells on the microplates and cell culture dish in parallel. The electrotaxis on the microplates was consistent with that on cell culture dishes (fig. S8).

Collective contribution of the TORC2/PKB and PI3K pathways to electrotaxis

The TORC2 pathway acts in parallel with PIP₃ (phosphatidylinositol 3,4,5-trisphosphate) to mediate the chemotactic response (*36*). To determine the relative contribution of the main parallel pathways underlying chemotaxis in electrotaxis, we compared mutants lacking components in the TORC2, PI3K, or PLA₂ (phospholipase A2) pathways. The *piaA⁻* cells had the most significantly decreased directedness value (~24% of wild-type cells). Cells treated with the PI3K inhibitor LY294002 also had markedly decreased directedness (~56% of controls). However, the *pla2⁻* cells displayed an electrotactic response comparable to that of

wild-type AX2 cells. *piaA⁻/pla2⁻* cells and LY294002-treated *piaA⁻/pla2⁻* cells displayed the most significantly decreased electrotactic response, with directedness values similar to that of *piaA⁻* cells, but the latter cells also displayed decreased motility (Fig. 5, A to D). To corroborate the role of the PI3K pathway, we examined a strain lacking PI3K1 and PI3K2 (*pi3k1⁻2⁻*). Consistent with the effect of LY294002 treatment, *pi3k1⁻2⁻* cells showed significantly decreased electrotaxis (Fig. 5, E and F). Together, these data suggest that chemotaxis and electrotaxis use largely overlapping signaling transduction pathways to affect the cytoskeleton, in that piaA and the TORC2/PKB pathways play predominant roles in these responses (Fig. 6).

DISCUSSION

We established a high-throughput approach to screen for genes and molecules that underlie electrotaxis. We used barcoded microplates and multifield time-lapse microscopy to achieve large-scale screening of a collection of *Dictyostelium* mutants. We identified four categories of electrotaxis phenotypes: wild type–like, moderately defective, severely defective, and hyperresponsive mutants. Focusing on the severely defective mutants, we found that PiaA was an essential mediator of electrotaxis, which we confirmed using knockout, pharmacological, and rescue experiments. Disruption of additional TORC2 components, as well as upstream and downstream molecules, suggested important roles for the TORC2 pathway in electrotaxis.

High-throughput techniques with increased efficiency to quantify electrotaxis phenotypes

Dictyostelium is a powerful model to identify molecular components involved in electrotaxis because of its motility, robust electrotaxis, and genetic tractability. Traditional electrotaxis experiments have used one chamber per cell type, which meant characterization of only one strain per experimental run. Although our method also used only one chamber, individual strains of cells were seeded on barcoded microplates, which enabled many strains to be placed into the chamber at once (fig. S2A). Here, we routinely used 30 different strains on predefined microplates per experimental run, representing a 30-fold increase in efficiency (fig. S2, B and C, and Fig. 1A). The capacity could easily be scaled up to 100 strains per run. The method offers a substantially higher screening efficiency and allowed us to identify defective and hyperresponsive mutants (Fig. 1, A to D). The discovery of hyperresponsive strains was intriguing because the enhanced response to an electric field did not always correlate with increased motility.

Signaling mechanisms in electrotaxis

Our finding that cell lines lacking PiaA or other components of the TORC2 complex as well as its upstream regulators and downstream substrates each display defects suggests an important role of this signaling cascade in electrotaxis. Further experiments are needed to determine
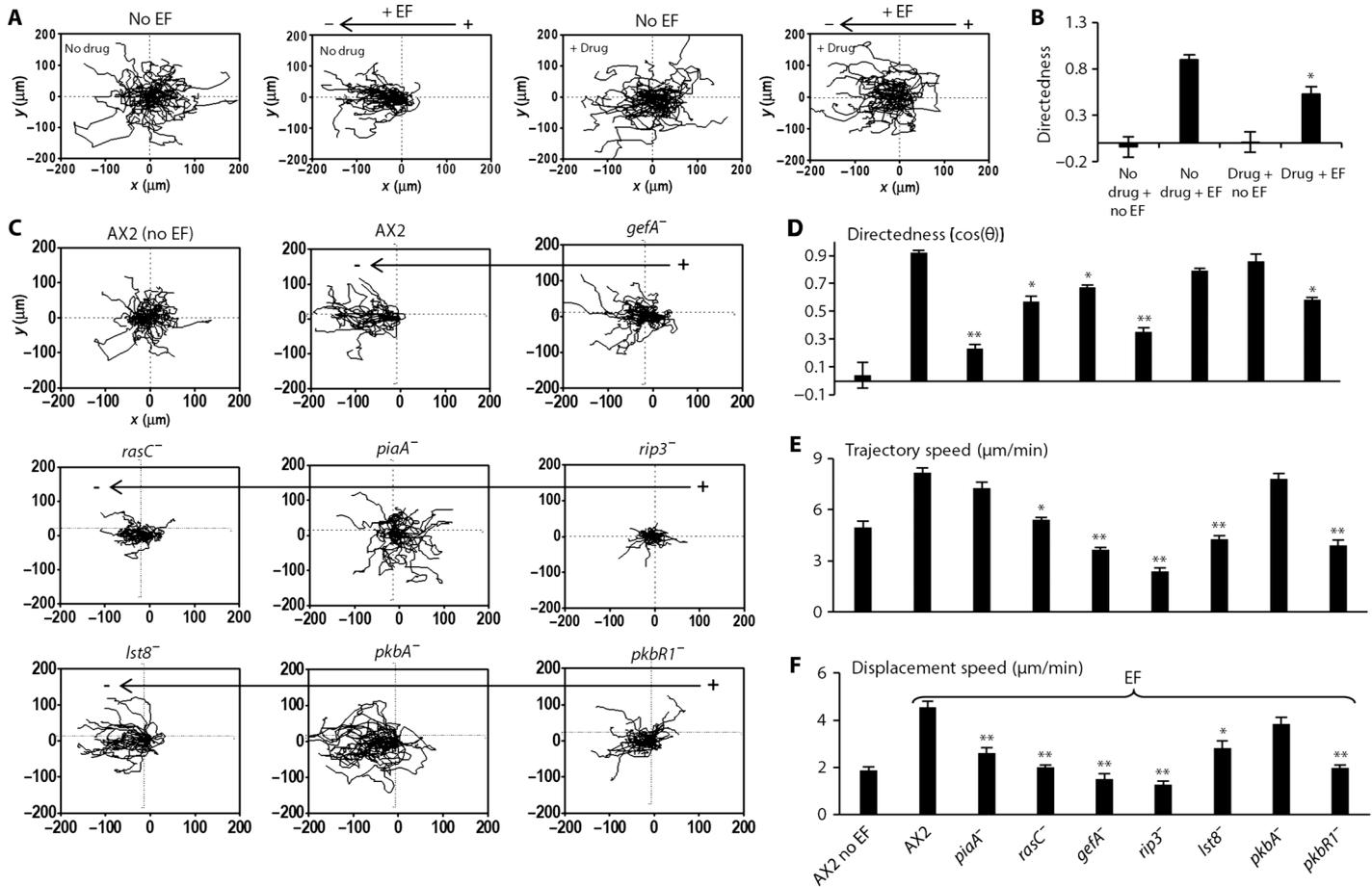
Fig. 4. The TORC2/PKB pathway in electrotaxis. (A and B) Pharmacological inhibition of TORC2-impaired electrotaxis, as shown by compiled cell migration trajectories (AX2) (A) and migration directedness values (B). Cells were treated with TORC2 inhibitor pp242 for 30 min before being exposed to an electric field of 12 V/cm in the continuous presence of the inhibitor. Data are means ± SEM from at least 50 cells per treatment from three independent experiments. *$P < 0.05$ when compared with no drug in an electric field. (C to F) Knockouts of components of TORC2 signaling pathway significantly affected electrotaxis, but to different extents on migration directedness and speed. Knockouts of components of TORC2 signaling pathway ($piaA^-$, $rasC^-$, $gefA^-$, $rip3^-$, and $pkbR1^-$) significantly reduced the directedness values (C and D) and differentially affected trajectory speed and displacement speed (E and F). Cell migration trajectories are presented with the start point of each cell set at the origin. WT cells (AX2) migrated directionally toward the cathode (to the left). Data are means ± SEM from 50 cells per treatment or per genotype in an electric field of 12 V/cm from three independent experiments. *$P < 0.05$, **$P < 0.01$, Student's t test, compared with AX2 WT cells in an electric field of the same strength.

whether the TORC2 pathway is important for sensing of the electric field or for cell motility, both of which are needed for electrotaxis. Although the disruption of *piaA* affected both directedness and motility, the effect on directedness was greater. In contrast, $lst8^-$ cells showed minimal defect in directedness but a mild decrease in migration speed (Fig. 4, D to F). The $rip3^-$ cells showed strong defects in both directedness and migration speed (Fig. 4, C to F). Because none of the mutants deficient in TORC2 pathway components displayed a defect purely in directedness, we cannot conclude that the pathway functions as the sensor of the electric field.

Chemotaxis studies in *Dictyostelium* and neutrophils have revealed a new paradigm for directed cell migration—the signal transduction network composed of sophisticated parallel pathways not only guide cells but also are the essential drivers of cell motility. Consistently, we found that the directedness and migration defects associated with cells lacking GefA, RasC, and PKBR1 were not as strong as the defects observed in

cells lacking PiaA and Rip3, indicating that additional upstream and downstream signaling molecules may also be involved (Fig. 6). Moreover, simultaneous disruption of multiple signaling pathways, including PI3K, TORC2/PKB, and PLA₂, resulted in cells with decreased motility and consequently with a severe defect in electrotaxis (Fig. 5A). Because signal transduction networks drive motility through regulation and feedback of the cytoskeletal network, we speculate that electric fields might bias the signaling transduction and cytoskeletal networks, which could be a point of integration of the two different external signals (Fig. 6).

Although the mechanisms for sensing chemical gradients and electric fields are likely different, chemotaxis and electrotaxis appear to share common regulatory circuits that control cell movement (Fig. 6). Future studies are needed to determine the extent of overlap between chemotaxis and electrotaxis and the molecule or molecules, equivalent to the chemoattractant receptors, which specifically sense the electric field. Our results provide interesting candidates for such investigation.

Fig. 5. Contribution of the TORC2/PKB, PI3K, and PLA$_2$ pathways to electrotaxis. (**A**) Roles of three chemotaxis pathways—TORC2/PKB, PIP$_3$, and PLA$_2$—in electrotaxis. PiaA and PI3K played more critical roles. Knockout or inhibition of three pathways that function in chemotaxis—TORC2/PKB, PIP$_3$, and PLA$_2$—eliminated electrotaxis. (**B** to **D**) Effect of knockout of pla2 (*pla2*⁻), double knockout of pla2 and piaA (*pla2*⁻/*piaA*⁻), or double knockout of pla2 and piaA and PI3K inhibition with LY294002 (LY) on cell migration directedness (B), trajectory speed (C), and displacement speed (D). (**E**) Cell migration trajectories are presented with the start point of each cell set at the origin. WT cells (AX2) migrated directionally toward the cathode (to the left). Electrotaxis was significantly impaired in *pi3k*⁻/⁻ cells (null mutation of *pi3k1* and *pi3k2*). (**F**) The PI3K knockout strain showed significantly decreased directedness values and decreased track speed and displacement speed. Migration trajectories of cells in an EF with the cathode on the left. The square is 200 μm × 200 μm. Polarity is as shown. Data are means ± SEM from 50 cells per genotype or per treatment in an electric field of 12 V/cm from three independent experiments. *$P < 0.05$, **$P < 0.01$, Student's *t* test, compared with AX2 WT cells.
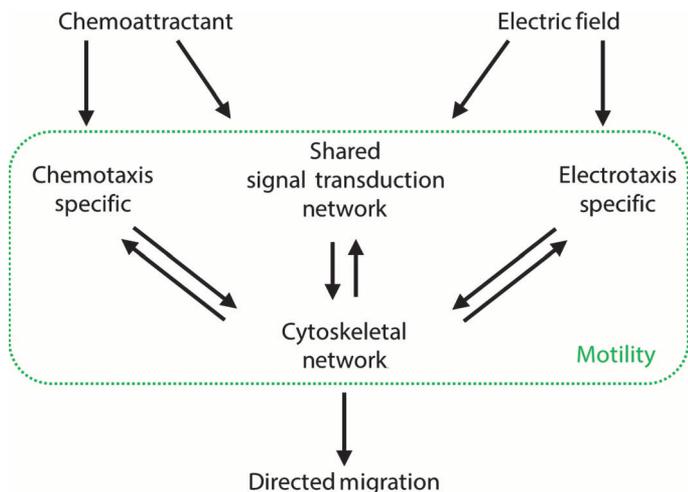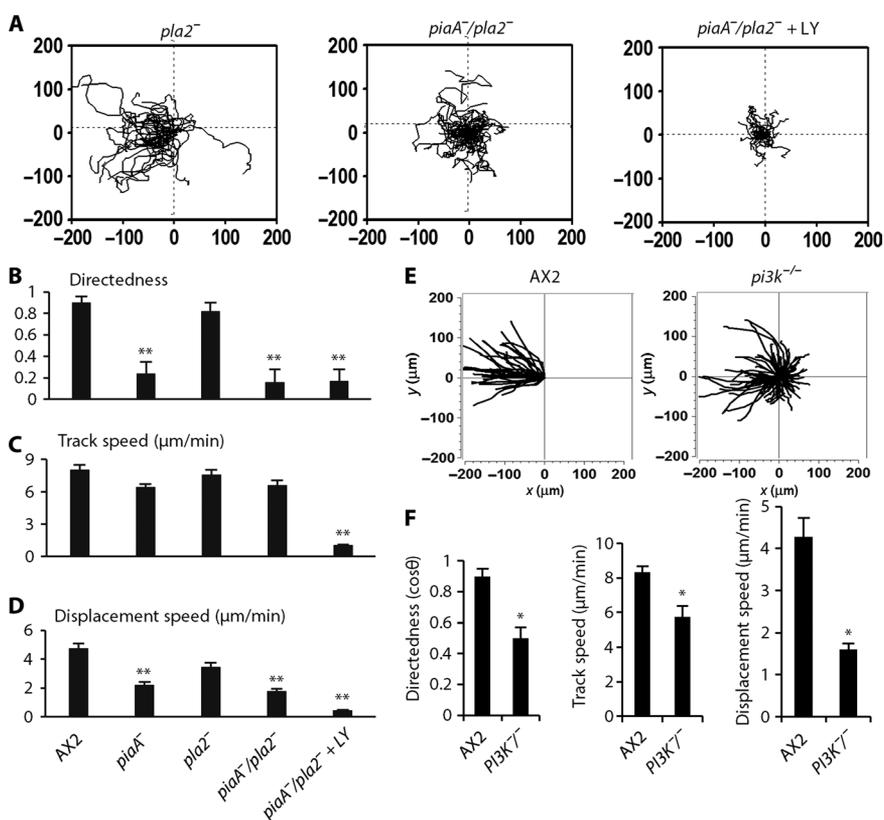

Fig. 6. Diagram depicting hypothetical mechanisms of electrotaxis against chemotaxis. The major signaling network (TORC2 and PI3K) appears to be shared between electrotaxis and chemotaxis. Some receptors, for example, the cAMP receptor cAR1 and downstream G protein Gβ, are essential for chemotaxis, but not for electrotaxis. This suggests that there are some chemotaxis- and electrotaxis-specific pathways. Electric fields activate the major shared signaling network and an as yet to be identified specific pathway that converge on the cytoskeletal network, which is altered during both chemotaxis and electrotaxis (green box). Changes in the cytoskeleton network result in cell motility and directed migration.

MATERIALS AND METHODS

REMI library and cell lines

We used a REMI vector, pBRS1, and the library was made in AX2 cells from R. Kay's laboratory. We selected colonies with blasticidin for 6 to 7 days. Colonies were collected and spread onto SM plates with bacterial cultures. The transformants appeared as pinpoint plaques in about 3 days and grew to form larger plaques over the following few days. Desired mutants with morphological defects were selected (fig. S1 and Table 1). Knockout constructs, pMYC32 and pYL23, were used to create the *piaA*⁻ mutants MYC15 and MYC28, respectively, by homologous recombination (*35*).

Design, materials, and fabrication for barcoded microplates

The microplates served as the substrate on which the cells attached and migrated. Each microplate carried a unique graphic barcode pattern, which was directly correlated with the type of mutant carried by the microplate and hence enabled easy mutant identification (fig. S3A). A square microplate design was used for its large migration area and easy barcode placement. An example of a microplate is shown with the graphic barcode of a 6-bit binary design, with one orientation bit indicating the front or backside of the plate and five information bits encoding the microplate (fig. S3B). With this 5-bit information code, we could encode $2^5 = 32$ different mutants. The encoding capacity could be increased by improving the photolithography resolution and using more complicated code design.

The barcoded microplates were fabricated using photolithography of a polyethylene glycol (PEG) hydrogel material. PEG hydrogel is a commonly used biomedical material because of its excellent biocompatibility,

optical transparency, flexibility, and resistance to nonspecific binding (*46*, *47*). PEG hydrogel has been routinely fabricated through ultraviolet (UV)–induced crosslinking process using vinyl-functionalized PEG building blocks, which enabled us to generate submillimeter microplates with micrometer graphic barcodes (*48*). The barcoded microplate fabrication started with the preparation of PEG prepolymer solution. It consisted of vinyl-terminated PEG (molecular weight, 700; 98%, v/v) and photoinitiator (2-hydroxyl-2-methylpropiophenone; 2%, v/v). The prepolymer solution was subsequently drop-dispensed on a photomask bearing the barcoded microplate patterns. The prepolymer solution was then covered by a glass coverslip and exposed to UV irradiation through the photomask, which defined the microplate and barcode patterns. Next, the coverslip with the barcoded microplates was separated from the photomask and thoroughly rinsed with ethanol. The microplates were then briefly treated with oxygen plasma to allow cell adhesion and migration. Eventually, the barcoded microplates were released from the coverslip, collected, and stored in 70% ethanol until use.

Cell culture and preparation for electrotaxis experiments

AX2 cells, AX3 (wild-type), and REMI mutants were grown in axenic HL5 medium [protease peptone (10 g/liter), yeast extract (5 g/liter), glucose (10 g/liter), Na_2HPO_4 (0.35 g/liter), KH_2PO_4 (0.35 g/liter), streptomycin sulfate (10 mg/ml), pH 6.4] at 22°C. Cells growing in log phase (~3×10^6 to 4×10^6 cells/ml) were washed once and starved in development buffer (DB; 5 mM Na_2HPO_4, 5 mM KH_2PO_4, 2 mM $MgSO_4$, and 0.2 mM $CaCl_2$) for 3 hours. TORC2 inhibitor pp242 was purchased from Tocris Bioscience (catalog no. 4257) and used at 50 μM. All procedures were carried out at room temperature (~22°C), unless otherwise indicated.

Loading developed cells on barcoded microplates

Barcoded microplates were stored in 70% ethanol and washed thoroughly with DB solution before loading cells. Cells were suspended and loaded onto defined barcoded microplates, which were presettled in a 24-well plate (different mutant and barcode in each well). After 10 min, nonadherent cells were gently washed away and the barcoded microplates were mixed up and moved into an electrotaxis chamber. Wild-type parental cells (AX2) were used in each experiment as the internal control. The five-digit binary barcode design allowed simultaneous seeding of hundreds of different strains of mutant. We normally used 30 types of microplates in each electrotaxis chamber, which is 30 times more efficient than conventional electrotaxis experiments.

Electrotaxis assays

Electrotaxis experiments were carried out as previously described (*5*, *20*, *49*). In brief, an electric field was applied for 30 min at indicated field strength through agar salt bridges. Multifield time-lapse images of cells on different coded plates were acquired using an inverted microscope (Axiovert 40, Carl Zeiss) equipped with a charge-coupled device camera (C4742-95; Hamamatsu Corporation) and a motorized XYZ stage (BioPoint 2, Ludl Electronic Products Ltd.) controlled by SimplePCI imaging software.

Molecular cloning of the site of insertion and the flanking DNA

The site of insertion was identified by directed cloning, using plasmid rescue. We isolated genomic DNA from the REMI insertion strain, which was digested with restriction enzyme Psi I overnight at 37°C. We then purified the digestion products by heating at 65°C for 40 min, followed by ligation using a Quick Ligation Kit. We then transformed competent Stbl4 cells by electroporation using 2 μl of the ligation reaction products. Plasmids of clones were extracted and sequenced, and the insertion regions were identified. A short sequence read from the insertion site usually identified the targeted gene in the database.

Gene disruption and transformation

We knocked out genes in wild-type cells using homologous recombination to confirm the phenotype. *piaA*⁻ cells were constructed in an AX2 background. We then reexpressed *Flag-tagged piaA* in *piaA*⁻ cells, transformed the construct into *piaA*⁻ cells by electroporation, and selected the cells in the presence of G418 (20 μg/ml) (*36*, *50*). Other knockouts and parental cells are listed in table S3.

Quantitative analysis of electrotaxis

Cell migration was recorded with a frame interval of 30 s using MetaMorph (Universal Imaging Corp.) and analyzed using ImageJ (National Institutes of Health). Trajectories of cells were pooled to make composite graphs (Fig. 1E). The electrotactic index (directedness) was used to quantify how directionally cells migrated in an electric field. To calculate the electrotactic index, the cosine of the angle between the direction of movement and the direction of electric vector was determined. The directedness of migration was assessed as cosine θ, in which θ is the angle between the electric field vector and a straight line connecting the start and end positions of a cell. A cell moving directly to the cathode would have a directedness of 1; a cell moving directly to the anode would have a directedness of −1. A value close to 0 represents random cell movement. The average directedness of a population of cells gives a quantification of how directionally cells have moved. For migration speed, we used trajectory speed (the total length traveled by the cells divided by time) and the displacement speed—the straight-line distance between the start and end positions of a cell, divided by time (*5*). Persistency was calculated as the shortest linear distance between the start and end points of the migration path (displacement distance) divided by the total distance traveled by a cell (trajectory length). A smaller value indicates a more wandering cell path, whereas a higher value shows more direct migration. All motile isolated cells were analyzed. A minimum of 40 cells or more as indicated from three independent experiments were analyzed.

Statistics

All data are presented as means ± SEM. The Student's *t* test (two-tailed) was used for statistical analysis, and a *P* value less than 0.05 was considered as statistically significant.

SUPPLEMENTARY MATERIALS

www.sciencesignaling.org/cgi/content/full/8/378/ra50/DC1
Fig. S1. The collection of mutant strains with morphological defects used in our screen.
Fig. S2. High-throughput screening strategy to determine electrotaxis phenotypes.
Fig. S3. Design and fabrication of the barcoded microplates.
Fig. S4. Cells on barcoded microplates at different positions in an electrotaxis chamber showed consistent electrotaxis responses.
Fig. S5. *Dictyostelium* cells displayed consistent migration phenotypes on both barcoded microplates and tissue culture dishes.
Fig. S6. Recapitulation of the defective electrotaxis phenotype in the mutant strains by knockout cells.
Fig. S7. Electrotaxis of vegetative cells.
Fig. S8. Mutated strains of *Dictyostelium* cells displayed consistent migration phenotypes on barcoded microplates and tissue culture dishes.
Table S1. Defective strains identified from the screen.
Table S2. Hyperresponsive strains identified.
Table S3. Knockouts confirmed the genes that underlie the 12 defective strains.
Movie S1. Wild-type AX2 cell not in an electric field.
Movie S2. Wild-type AX2 cell in an electric field of 12 V/cm.
Movie S3. PiaA⁻ in an electric field of 12 V/cm.
Movie S4. Reexpression of piaA in *piaA*⁻ cells restored electrotaxis.

REFERENCES AND NOTES

1. J. D. Anderson, Galvanotaxis of slime mold. *J. Gen. Physiol.* **35**, 1–16 (1951).
2. N. Ogawa, H. Oku, K. Hashimoto, M. Ishikawa, A physical model for galvanotaxis of *Paramecium* cell. *J. Theor. Biol.* **242**, 314–328 (2006).

3. M. Verworn, Untersuchungen über die polare Erregung der lebendigen Substanz durch den konstanten Strom. *Arch. Gesamte Physiol. Menschen Tiere* **62**, 415–450 (1896).

4. W. Seifriz, A theory of protoplasmic streaming. *Science* **86**, 397–398 (1937).

5. M. Zhao, T. Jin, C. D. McCaig, J. V. Forrester, P. N. Devreotes, Genetic analysis of the role of G protein–coupled receptor signaling in electrotaxis. *J. Cell Biol.* **157**, 921–927 (2002).

6. L. Hinkle, C. D. McCaig, K. R. Robinson, The direction of growth of differentiating neurones and myoblasts from frog embryos in an applied electric field. *J. Physiol.* **314**, 121–135 (1981).

7. R. J. Cork, M. E. McGinnis, J. Tsai, K. R. Robinson, The growth of PC-12 neurites is biased towards the anode of an applied electrical field. *J. Neurobiol.* **25**, 1509–1516 (1994).

8. D. M. Graham, L. Huang, K. R. Robinson, M. A. Messerli, Epidermal keratinocyte polarity and motility require Ca^{2+} influx through TRPV1. *J. Cell Sci.* **126**, 4602–4613 (2013).

9. Y. J. Huang, J. Samorajski, R. Kreimer, P. C. Searson, The influence of electric field and confinement on cell motility. *PLOS One* **8**, e59447 (2013).

10. H. Y. Yang, R. P. Charles, E. Hummler, D. L. Baines, R. R. Isseroff, The epithelial sodium channel mediates the directionality of galvanotaxis in human keratinocytes. *J. Cell Sci.* **126**, 1942–1951 (2013).

11. F. Chang, N. Minc, Electrochemical control of cell and tissue polarity. *Annu. Rev. Cell Dev. Biol.* **30**, 317–336 (2014).

12. A. Haupt, A. Campetelli, D. Bonazzi, M. Piel, F. Chang, N. Minc, Electrochemical regulation of budding yeast polarity. *PLOS Biol.* **12**, e1002029 (2014).

13. D. M. Thompson, A. N. Koppes, J. G. Hardy, C. E. Schmidt, Electrical stimuli in the central nervous system microenvironment. *Annu. Rev. Biomed. Eng.* **16**, 397–430 (2014).

14. M. S. Kim, M. H. Lee, B. J. Kwon, H. J. Seo, M. A. Koo, K. E. You, D. Kim, J. C. Park, Control of neonatal human dermal fibroblast migration on poly(lactic-co-glycolic acid)-coated surfaces by electrotaxis. *J. Tissue Eng. Regen. Med.* 10.1002/term.1986 (2015).

15. K. Y. Nishimura, R. R. Isseroff, R. Nuccitelli, Human keratinocytes migrate to the negative pole in direct current electric fields comparable to those measured in mammalian wounds. *J. Cell Sci.* **109** (Pt. 1), 199–207 (1996).

16. M. Zhao, A. Agius-Fernandez, J. V. Forrester, C. D. McCaig, Orientation and directed migration of cultured corneal epithelial cells in small electric fields are serum dependent. *J. Cell Sci.* **109** (Pt. 6), 1405–1414 (1996).

17. L. F. Jaffe, R. Nuccitelli, An ultrasensitive vibrating probe for measuring steady extracellular currents. *J. Cell Biol.* **63**, 614–628 (1974).

18. J. Pu, M. Zhao, Golgi polarization in a strong electric field. *J. Cell Sci.* **118**, 1117–1128 (2005).

19. H. Bai, C. D. McCaig, J. V. Forrester, M. Zhao, DC electric fields induce distinct preangiogenic responses in microvascular and macrovascular cells. *Arterioscler. Thromb. Vasc. Biol.* **24**, 1234–1239 (2004).

20. B. Song, Y. Gu, J. Pu, B. Reid, Z. Zhao, M. Zhao, Application of direct current electric fields to cells and tissues in vitro and modulation of wound electric field in vivo. *Nat. Protoc.* **2**, 1479–1489 (2007).

21. M. Zhao, B. Song, J. Pu, T. Wada, B. Reid, G. Tai, F. Wang, A. Guo, P. Walczysko, Y. Gu, T. Sasaki, A. Suzuki, J. V. Forrester, H. R. Bourne, P. N. Devreotes, C. D. McCaig, J. M. Penninger, Electrical signals control wound healing through phosphatidylinositol-3-OH kinase–γ and PTEN. *Nature* **442**, 457–460 (2006).

22. R. Nuccitelli, P. Nuccitelli, C. Li, S. Narsing, D. M. Pariser, K. Lui, The electric field near human skin wounds declines with age and provides a noninvasive indicator of wound healing. *Wound Repair Regen.* **19**, 645–655 (2011).

23. R. Nuccitelli, P. Nuccitelli, S. Ramlatchan, R. Sanger, P. J. Smith, Imaging the electric field associated with mouse and human skin wounds. *Wound Repair Regen.* **16**, 432–441 (2008).

24. A. T. Barker, L. F. Jaffe, J. W. Vanable Jr., The glabrous epidermis of cavies contains a powerful battery. *Am. J. Physiol.* **242**, R358–R366 (1982).

25. R. Nuccitelli, M. M. Poo, L. F. Jaffe, Relations between ameboid movement and membrane-controlled electrical currents. *J. Gen. Physiol.* **69**, 743–763 (1977).

26. B. Reid, R. Nuccitelli, M. Zhao, Non-invasive measurement of bioelectric currents with a vibrating probe. *Nat. Protoc.* **2**, 661–669 (2007).

27. G. M. Allen, A. Mogilner, J. A. Theriot, Electrophoresis of cellular membrane components creates the directional cue guiding keratocyte galvanotaxis. *Curr. Biol.* **23**, 560–568 (2013).

28. Y. Sun, H. Do, J. Gao, R. Zhao, M. Zhao, A. Mogilner, Keratocyte fragments and cells utilize competing pathways to move in opposite directions in an electric field. *Curr. Biol.* **23**, 569–574 (2013).

29. M. Zhao, A. Dick, J. V. Forrester, C. D. McCaig, Electric field–directed cell motility involves up-regulated expression and asymmetric redistribution of the epidermal growth factor receptors and is enhanced by fibronectin and laminin. *Mol. Biol. Cell* **10**, 1259–1276 (1999).

30. M. B. A. Djamgoz, M. Mycielska, Z. Madeja, S. P. Fraser, W. Korohoda, Directional movement of rat prostate cancer cells in direct-current electric field: Involvement of voltagegated Na⁺ channel activity. *J. Cell Sci.* **114**, 2697–2705 (2001).

31. C. E. Pullar, B. S. Baier, Y. Kariya, A. J. Russell, B. A. Horst, M. P. Marinkovich, R. R. Isseroff, β4 integrin and epidermal growth factor coordinately regulate electric field-mediated directional migration via Rac1. *Mol. Biol. Cell* **17**, 4925–4935 (2006).

32. R. Nuccitelli, T. Smart, J. Ferguson, Protein kinases are required for embryonic neural crest cell galvanotaxis. *Cell Motil. Cytoskeleton* **24**, 54–66 (1993).

33. M. J. Sato, M. Ueda, H. Takagi, T. M. Watanabe, T. Yanagida, M. Ueda, Input–output relationship in galvanotactic response of *Dictyostelium* cells. *Biosystems* **88**, 261–272 (2007).

34. M. J. Sato, H. Kuwayama, W. N. van Egmond, A. L. Takayama, H. Takagi, P. J. van Haastert, T. Yanagida, M. Ueda, Switching direction in electric-signal-induced cell migration by cyclic guanosine monophosphate and phosphatidylinositol signaling. *Proc. Natl. Acad. Sci. U.S.A.* **106**, 6667–6672 (2009).

35. M. Y. Chen, Y. Long, P. N. Devreotes, A novel cytosolic regulator, Pianissimo, is required for chemoattractant receptor and G protein-mediated activation of the 12 transmembrane domain adenylyl cyclase in *Dictyostelium. Genes Dev.* **11**, 3218–3231 (1997).

36. H. Cai, S. Das, Y. Kamimura, Y. Long, C. A. Parent, P. N. Devreotes, Ras-mediated activation of the TORC2–PKB pathway is critical for chemotaxis. *J. Cell Biol.* **190**, 233–245 (2010).

37. A. Kuspa, W. F. Loomis, Tagging developmental genes in *Dictyostelium* by restriction enzyme-mediated integration of plasmid DNA. *Proc. Natl. Acad. Sci. U.S.A.* **89**, 8803–8807 (1992).

38. A. Kuspa, Restriction enzyme-mediated integration (REMI) mutagenesis. *Methods Mol. Biol.* **346**, 201–209 (2006).

39. Y. Artemenko, K. F. Swaney, P. N. Devreotes, Assessment of development and chemotaxis in *Dictyostelium discoideum* mutants. *Methods Mol. Biol.* **769**, 287–309 (2011).

40. B. Apsel, J. A. Blair, B. Gonzalez, T. M. Nazif, M. E. Feldman, B. Aizenstein, R. Hoffman, R. L. Williams, K. M. Shokat, Z. A. Knight, Targeted polypharmacology: Discovery of dual inhibitors of tyrosine and phosphoinositide kinases. *Nat. Chem. Biol.* **4**, 691–699 (2008).

41. K. F. Swaney, C. H. Huang, P. N. Devreotes, Eukaryotic chemotaxis: A network of signaling pathways controls motility, directional sensing, and polarity. *Annu. Rev. Biophys.* **39**, 265–289 (2010).

42. P. G. Charest, Z. Shen, A. Lakoduk, A. T. Sasaki, S. P. Briggs, R. A. Firtel, A Ras signaling complex controls the RasC-TORC2 pathway and directed cell migration. *Dev. Cell* **18**, 737–749 (2010).

43. L. Liu, S. Das, W. Losert, C. A. Parent, mTORC2 regulates neutrophil chemotaxis in a cAMP- and RhoA-dependent fashion. *Dev. Cell* **19**, 845–857 (2010).

44. S. Lee, F. I. Comer, A. Sasaki, I. X. McLeod, Y. Duong, K. Okumura, J. R. Yates III, C. A. Parent, R. A. Firtel, TOR complex 2 integrates cell movement during chemotaxis and signal relay in *Dictyostelium. Mol. Biol. Cell* **16**, 4572–4583 (2005).

45. L. Liu, C. A. Parent, Review series: TOR kinase complexes and cell migration. *J. Cell Biol.* **194**, 815–824 (2011).

46. N. A. Alcantar, E. S. Aydil, J. N. Israelachvili, Polyethylene glycol–coated biocompatible surfaces. *J. Biomed. Mater. Res.* **51**, 343–351 (2000).

47. J. A. Hubbell, Biomaterials in tissue engineering. *Biotechnology* **13**, 565–576 (1995).

48. A. Revzin, R. J. Russell, V. K. Yadavalli, W. G. Koh, C. Deister, D. D. Hile, M. B. Mellott, M. V. Pishko, Fabrication of poly(ethylene glycol) hydrogel microstructures using photolithography. *Langmuir* **17**, 5440–5447 (2001).

49. M. Zhao, A. Agius-Fernandez, J. V. Forrester, C. D. McCaig, Directed migration of corneal epithelial sheets in physiological electric fields. *Invest. Ophthalmol. Vis. Sci.* **37**, 2548–2558 (1996).

50. M. Tang, M. Iijima, Y. Kamimura, L. Chen, Y. Long, P. Devreotes, Disruption of PKB signaling restores polarity to cells lacking tumor suppressor PTEN. *Mol. Biol. Cell* **22**, 437–447 (2011).

A large-scale screen reveals genes that mediate electrotaxis in
Dictyostelium discoideum

Runchi Gao, Siwei Zhao, Xupin Jiang, Yaohui Sun, Sanjun Zhao,
Jing Gao, Jane Borleis, Stacey Willard, Ming Tang, Huaqing Cai,
Yoichiro Kamimura, Yuesheng Huang, Jianxin Jiang, Zunxi Huang,
Alex Mogilner, Tingrui Pan, Peter N. Devreotes and Min Zhao (May
26, 2015)

The following resources related to this article are available online at http://stke.sciencemag.org.
This information is current as of May 26, 2015.

Article Tools	Visit the online version of this article to access the personalization and article tools: http://stke.sciencemag.org/content/8/378/ra50
Supplemental Materials	*"Supplementary Materials"* http://stke.sciencemag.org/content/suppl/2015/05/21/8.378.ra50.DC1.html
Related Content	The editors suggest related resources on *Science*'s sites: http://stke.sciencemag.org/content http://www.sciencemag.org/content/sci/324/5925/384.full.html http://stm.sciencemag.org/content/scitransmed/6/265/265sr6.full.html http://stke.sciencemag.org/content/sigtrans/8/378/pc13.full.html
References	This article cites 49 articles, 22 of which you can access for free at: http://stke.sciencemag.org/content/8/378/ra50#BIBL
Glossary	Look up definitions for abbreviations and terms found in this article: http://stke.sciencemag.org/cgi/glossarylookup
Permissions	Obtain information about reproducing this article: http://www.sciencemag.org/about/permissions.dtl